Journal of Alloys and Compounds 508 (2010) 554–558

Contents lists available at ScienceDirect

Journal of Alloys and Compounds

journal homepage: www.elsevier.com/locate/jallcom

# Preparation and characterization of nanocrystalline $Mg_2FeH_6$

Yan Wang, Fangyi Cheng, Chunsheng Li, Zhanliang Tao, Jun Chen*

*Institute of New Energy Material Chemistry and Key Laboratory of Advanced Energy Materials Chemistry (Ministry of Education), Nankai University, Tianjin 300071, PR China*

ARTICLE INFO

*Article history:*
Received 4 June 2010
Received in revised form 8 August 2010
Accepted 13 August 2010
Available online 28 September 2010

*Keywords:*
Nanocrystalline $Mg_2FeH_6$
Ball milling
Rietveld refinement
Hydrogen storage
Desorption

ABSTRACT

We report on the preparation and characterization of nanocrystalline $Mg_2FeH_6$ that is prepared by ball milling of 3Mg + Fe mixture under relatively lower hydrogen pressure (5.5 bar) at room temperature. The phase, composition and morphology of the as-milled powders are characterized by X-ray diffraction (XRD), Transmission electron microscope (TEM) and high-resolution TEM (HRTEM). The results show that the optimum formation time of $Mg_2FeH_6$ phase is 100 h and the abundance is about 90.1 wt% deduced from Reitveld refinement. Together with $Mg_2FeH_6$, small amount of Fe and MgO are also present in the milled product. The as-prepared nanocrystalline $Mg_2FeH_6$, which exhibits a chrysanthemum-like spherical shape (Ø 100–200 nm) with aggregated nanoparticles (Ø 10–20 nm), starts to desorb hydrogen at 335 K and ends at 613 K with a total weight loss of 5.15 wt%. The desorption enthalpy and entropy for the as-prepared nanocrystalline $Mg_2FeH_6$ are $-67.2 \pm 8$ kJ/mol $H_2$ and $-120.1 \pm 15$ J/K mol $H_2$, respectively.


## 1. Introduction

Mg-based transition-metal complex hydrides such as $Mg_2NiH_4$, $Mg_2CoH_5$, and $Mg_2FeH_6$, which have been rationalized by the 18-electron counting rules, have been considered as promising hydrogen-storage materials due to their high hydrogen capacity (gravimetric 5.47 wt% hydrogen and volumetric 150 kg $H_2$ $m^{-3}$) and low cost [1–5]. The preparation of $Mg_2FeH_6$ becomes a rather difficult task and has attracted much attention. The reason is that $Mg_2FeH_6$ cannot be accomplished by directly hydrogenation of the binary alloys, since neither the dehydrogenated intermetallic compound (i.e., $Mg_2Fe$) nor stable alloy between Mg and Fe exists [6]. In 1984, Didisheim et al. reported for the first time the preparation of $Mg_2FeH_6$ by sintering 2Mg + Fe powders at elevated temperature of 723–793 K and hydrogen pressure of 20–120 bar for 2–10 days [7]. Selvam et al. demonstrated that the as-prepared sample by sintering at hydrogen pressure of 20–120 bar still contained up to 50% of non-reacted elements [8]. In the meantime, the mechanical alloying that is mainly based on milling of Mg + Fe or $MgH_2$ + Fe mixture under different hydrogen pressure from about 10 to 100 bar has been applied to prepare $Mg_2FeH_6$ at mild temperature [9–13]. For example, Varin et al. reported that the yield of $Mg_2FeH_6$ was 57 wt% after continuous mechanical alloying for 270 h under a hydrogen atmosphere at 8.8 bar [11]. Sai Raman et al. displayed that for 2Mg + Fe mixture, milling under hydrogen (10 bar) produced 63% $Mg_2FeH_6$ excluding oxides [12]. George et al. reported a yield of 84 wt% $Mg_2FeH_6$ phase through mechanical alloying of $2MgH_2$ + Fe mixture for 72 h followed by sintering at 673 K under a hydrogen atmosphere at 100 bar [13]. From previous literatures [9–14], it can be seen that lowering the hydrogen pressure during the mechanical alloying or sintering and increasing the purity of $Mg_2FeH_6$ are needed. Furthermore, it is also obviously to raise the questions that follow: (1) How large is the crystalline size during the phase change through the mechanical alloying; (2) The amorphous phase is generally described for the long-time ball milling (or mechanical alloying), while are there nanocrystals in the as-prepared samples and if yes, what is the effect on the hydrogen desorption. Therefore, to lower the hydrogen pressure during the preparation process and to increase the proportion of $Mg_2FeH_6$ in the synthesized product, we here report on the preparation of nanocrystalline $Mg_2FeH_6$ with high proportion and regular morphology by ball milling under relatively low hydrogen pressure. Interestingly, the as-prepared nanocrystalline $Mg_2FeH_6$ desorbs hydrogen at 335 K with a total weight loss of 5.15 wt% at the ending of 613 K.

## 2. Experimental details

### 2.1. Synthesis

Magnesium powder (purity of 99.99%, 0.5–1 μm) and iron powder (purity of 99.96%, 50–100 nm) were mixed in a 3Mg:Fe atomic ratio and milled in a Fritsch P7 planetary with operating at a rotation velocity of 320 rpm. Excessive Mg was subjected to the milling system because of the easy loss of Mg caused by adhering and cold-welding to the balls and the vial walls. The weight ratio between the ball and powder is 40:1. High–purity hydrogen (7 N) of 5.5 bar was introduced into the vial through a connection valve. The milling was carried out for 110 h. At regular intervals, a small amount of powder was taken out for phase analysis. All material handing (including weighing and loading) was carried out in a glove box under an

* Corresponding author. Tel.: +86 22 23502604; fax: +86 22 23502604.
*E-mail address:* chenabc@nankai.edu.cn (J. Chen).

0925-8388/$ – see front matter © 2010 Elsevier B.V. All rights reserved.
doi:10.1016/j.jallcom.2010.08.119

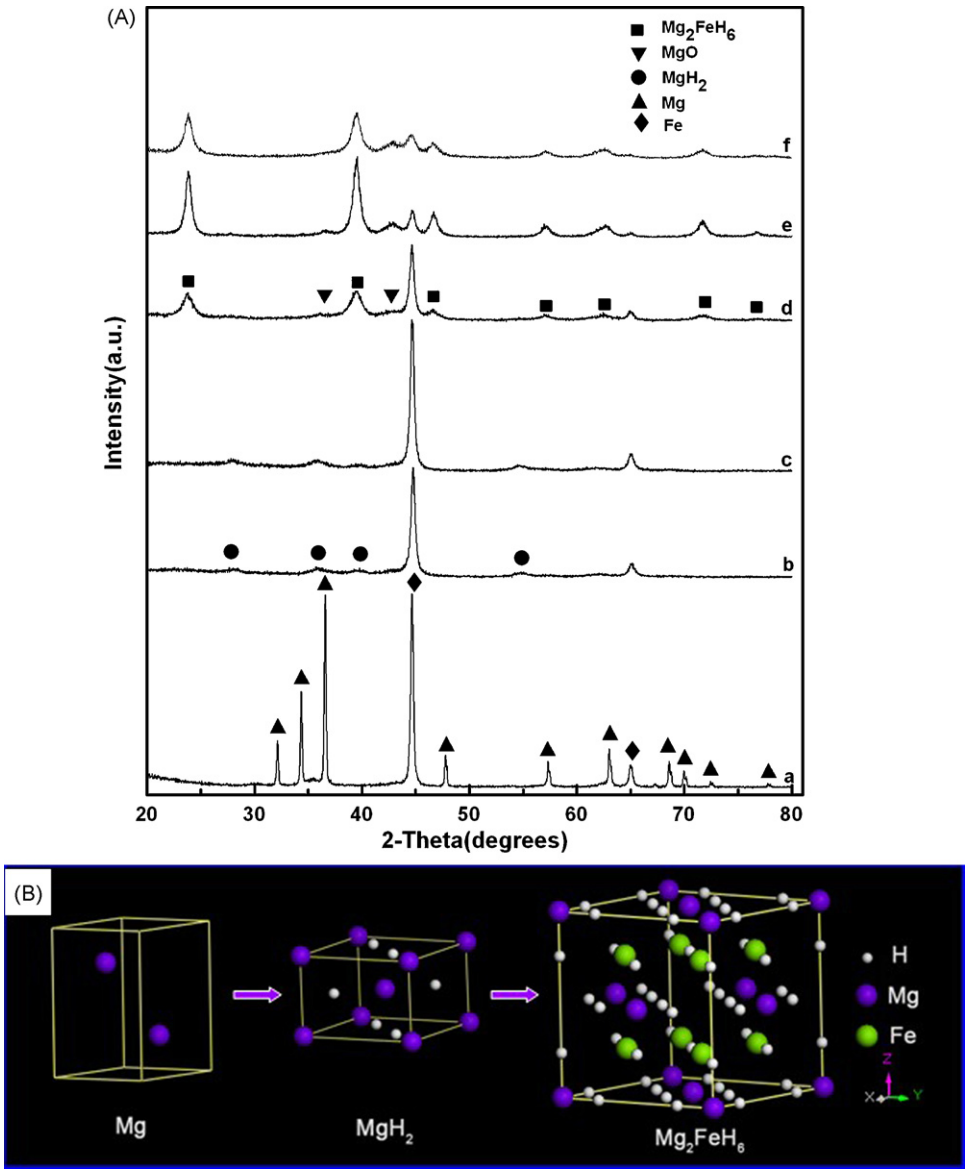


**Fig. 1.** (A) Powder XRD patterns of 3Mg + Fe mixture as a function of milling time: (a) 0 h, (b) 20 h, (c) 60 h, (d) 80 h, (e) 100 h and (f) 110 h at the hydrogen pressure of 5.5 bar. (B) Structural model sketch of the phase transformation from Mg to $MgH_2$ and then to $Mg_2FeH_6$.

inert pure argon (99.999%) atmosphere so as to minimize the contamination effect of oxygen and water on the sample.

### 2.2. Characterization

Powder X-ray diffraction (XRD) patterns were taken on a Rigaku-Dmax 2500 X-ray diffractometer using Cu Kα radiation (λ = 1.541 78 Å). The X-ray intensity was measured over a diffraction angle from 20° to 80° with a velocity of 0.02° per step. Rietveld refinement was performed to determine the phase composition and abundance of the as-milled powders using the Rietan-2000 program [15]. Transmission electron microscope (TEM) and high-resolution TEM (HRTEM) analyses were performed on a Philips Tecnai F 20 field emission TEM using an accelerating voltage of 200 kV. Thermogravimetry (TG) measurement was carried out by using computer controlled Hiden Isochema analyzer (IGA 001, Hiden Analytical Ltd) under vacuum. The pressure–composition–temperature (P–C–T) curves for hydrogen absorption and desorption were determined by using a computer controlled "Gas Reaction Controller" apparatus (PCT-2008, Shanghai).

## 3. Results and discussion

### 3.1. XRD analyses

Fig. 1A shows a series of powder X-ray diffraction (XRD) patterns of the as-milled samples obtained at different milling time. It can be seen that the phase composition has been greatly changed after ball milling. By inspecting the XRD pattern of the initial 3Mg + Fe mixture, the presence of metallic Mg and Fe can be readily identified. After 20 h of milling, the Mg precursor has nearly disappeared and new peaks arise, indicating the formation of $MgH_2$ phase (Joint Committee on Powder Diffraction Standards (JCPDS) No. 12-0697). Further ball milling up to 60 h does not significantly change the phase distribution, whereas the peak intensity ascribed to $MgH_2$ and Fe decreases obviously after 80 h. The milling finally results in the formation of a new hydride phase $Mg_2FeH_6$ (JCPDS No. 75-0675). Accordingly, the preparation of $Mg_2FeH_6$ in this study involves the following two-step reactions.

By comparison, for prolonged milling, there is no further increase of the peak intensity. In addition to $Mg_2FeH_6$, the presence of MgO and the remaining unreacted Fe can be observed in the final product. It can be seen that the peak intensity ascribed to $MgH_2$ and Fe decreases obviously, and the milling results in the formation of a new hydride phase $Mg_2FeH_6$ after 80 h. Further ball milling to 100 h, the peak of $MgH_2$ disappears, the peak intensity of $Mg_2FeH_6$ increases and there are distinguishable peaks of MgO.

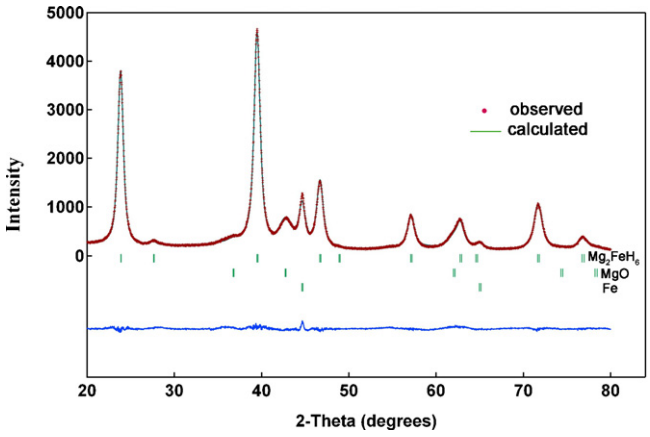


**Fig. 2.** Observed XRD pattern (red solid circles) and calculated profile (green solid lines) from Rietveld refinement of the product obtained by ball milling the 3Mg + Fe mixture for 100 h at the hydrogen pressure of 5.5 bar. Short vertical bars indicate the Bragg reflections of each fitted phase, as marked for $Mg_2FeH_6$, MgO and Fe. The bottom blue line is the difference between observed pattern and Rietveld refinement. (For interpretation of the references to color in this figure legend, the reader is referred to the web version of the article.)

From the above XRD patterns, we can infer that there are two kinds of trends for $MgH_2$, one is consumed to form $Mg_2FeH_6$ and the other is ascribed to MgO. Thus, it could conclude that MgO possibly originates from the reaction of highly active $MgH_2$ (rather than Mg) and polluted oxygen in the preparation process (especially during periodic extraction of powders).

The structure model sketch of the phase transformation from Mg to $Mg_2FeH_6$ is illustrated in Fig. 1B. First, hydrogen sorption on Mg matrix causes the $MgH_2$ intermediate product with tetragonal structure at stoichiometry ratio 1:2 (Mg:H). Subsequently, the reaction of $MgH_2$ and Fe at hydrogen atmosphere forms the $Mg_2FeH_6$ phase with cubic symmetry, showing the regular octahedral $FeH_6$ group surrounded by eight Mg atoms in a cubic configuration of $Mg_2FeH_6$.

$$Mg(s) + H_2(g) \rightarrow MgH_2(s) \quad (1)$$

$$2MgH_2(s) + Fe(s) + H_2(g) \rightarrow Mg_2FeH_6(s) \quad (2)$$

### 3.2. Rietveld refinement

In order to determine the phase composition and abundance of the as-milled powders, Rietveld refinement has been performed to analyze the XRD data using the Rietan-2000 program. Fig. 2 shows the observed XRD pattern, calculated pattern, and the difference between the observed and the calculated pattern by Rietveld refinement. The refinement results are listed in Table 1. The quite low $R$-weighted pattern ($R_{wp}$) and goodness fit ($S$) indicate the reliability of the refined output [16]. The refinement confirms that the as-milled product contains a single hydride phase $Mg_2FeH_6$, residual Fe and a small amount of MgO. The refined lattice parameter is found to be $a = 6.4424(1)$ Å for the cubic $Mg_2FeH_6$, in good agreement with earlier reports [17].

**Table 1**
Lattice parameter and phase abundance of the as-milled powders deduced from Rietveld refinement of XRD data.

| Phase | $Mg_2FeH_6$ | MgO | Fe |
|---|---|---|---|
| Crystal symmetry | Cubic | Cubic | Cubic |
| Lattice parameter (Å) | $a = 6.4424(1)$ | $a = 4.2211(4)$ | $a = 2.8686(2)$ |
| Abundance (wt%) | 90.1 | 4.0 | 5.9 |

$R_{wp} = 5.34$, $S = 1.15$

### 3.3. TEM and HRTEM analyses

Transmission electron microscope (TEM) and high-resolution TEM (HRTEM) analyses have been carried out to characterize the structure of the obtained product. Fig. 3a shows the representative TEM image of the as-prepared powders milled for 100 h. It can be observed that the product exhibits a chrysanthemum-like spherical shape with diameters of 100–200 nm with aggregated nanoparticles. The TEM image in Fig. 3b reveals that the spheres are composed of aggregated nanoparticles (10–20 nm). Such regular morphology might be caused by the existence of the residual Fe, which affords magnetic attraction for the assembly of nanoparticles. In order to obtain the detailed structural information, HRTEM has been performed (Fig. 3c). The observed interplanar distance of 0.278, 0.213, and 0.204 nm can be attributed to the (2 2 0) plane of $Mg_2FeH_6$, the (2 0 0) plane of MgO, and the (1 1 0) plane of Fe, respectively. This result confirms a mixed $Mg_2FeH_6$–MgO–Fe nanocrystalline structure, agreeing with the XRD analysis. Fig. 3d further shows the HRTEM image of an individual $Mg_2FeH_6$ nanoparticle along a different orientation, which is present in spherical shape with particle size of approximately 10 nm. The mutually perpendicular lattice fringes correspond to the (2 2 −1) and (0 1 −1) plane of $Mg_2FeH_6$, respectively. The corresponding fast Fourier transform (FFT) pattern (inset of Fig. 3d) can be well indexed to the cubic $Mg_2FeH_6$ being viewed down the [1 1 1] axis.

### 3.4. Hydrogen-storage properties

To determine the desorption of the as-prepared nanocrystalline $Mg_2FeH_6$, the TG analysis has been performed on an intelligent Gravimetric Analyzer (IGA 001, Hiden Isochema) under vacuum (Fig. 4). Obviously, the milled sample delivers two distinguished steps of mass loss. The first desorption starts at 335 K and ends at 521 K with a mass loss of approximately 0.75 wt%, corresponding to the decomposition of $Mg_2FeH_6$ as summarized in Eq. (3). It should be pointed out that the reaction is incompletely because of the low temperature. When the temperature is increased from 521 to 613 K, the sample loses weight of approximately 4.40 wt%, which is attributed to the integrated effects of Eqs. (3) and (4) (not one). The XRD curve for the dehydrogenated $Mg_2FeH_6$ has been showed in Fig. 5, and it can be seen that the final product is composed of Mg, Fe and some residual MgO. The total mass loss is 5.15 wt%, which should be from the hydrogen release of $Mg_2FeH_6$ phase in the milled product, since the involved other components (i.e., MgO and Fe) are inactive under the testing condition. Compared to the theoretical 5.47 wt% hydrogen content of $Mg_2FeH_6$, it can be inferred that the abundance of $Mg_2FeH_6$ phase is 94.1 wt%, which is slightly higher than the value determined from the Rietveld refinement of XRD. The high abundance of targeted $Mg_2FeH_6$ is attributed to the use of nanoscaled Fe as the precursor, which provides higher reactivity with the intermediate $MgH_2$, in comparison with bulk Fe commonly used in previous synthesis.

$$Mg_2FeH_6(s) \rightarrow 2MgH_2(s) + Fe(s) + H_2(g) \quad (3)$$

$$MgH_2(s) \rightarrow Mg(s) + H_2(g) \quad (4)$$

Fig. 6 shows the P–C–T curves in the first cycle of the obtained nanocrystalline $Mg_2FeH_6$ at 573, 548 and 523 K, respectively. All the P–C–T curves were measured without any activation process. Around hydrogen content of 2.5 wt%, the curves for both dehydrogenation and hydrogenation are uncommon, possibly due to the combination of simultaneously dehydriding and hydriding of the multiphases. From Fig. 6, it can also be seen that rehydrogenation of Mg + Fe + $H_2$ to form $Mg_2FeH_6$ is possible.

We take the hydrogen pressure at the point of hydrogen content 1.5 wt% as the desorption plateau, giving the data of (573 K,

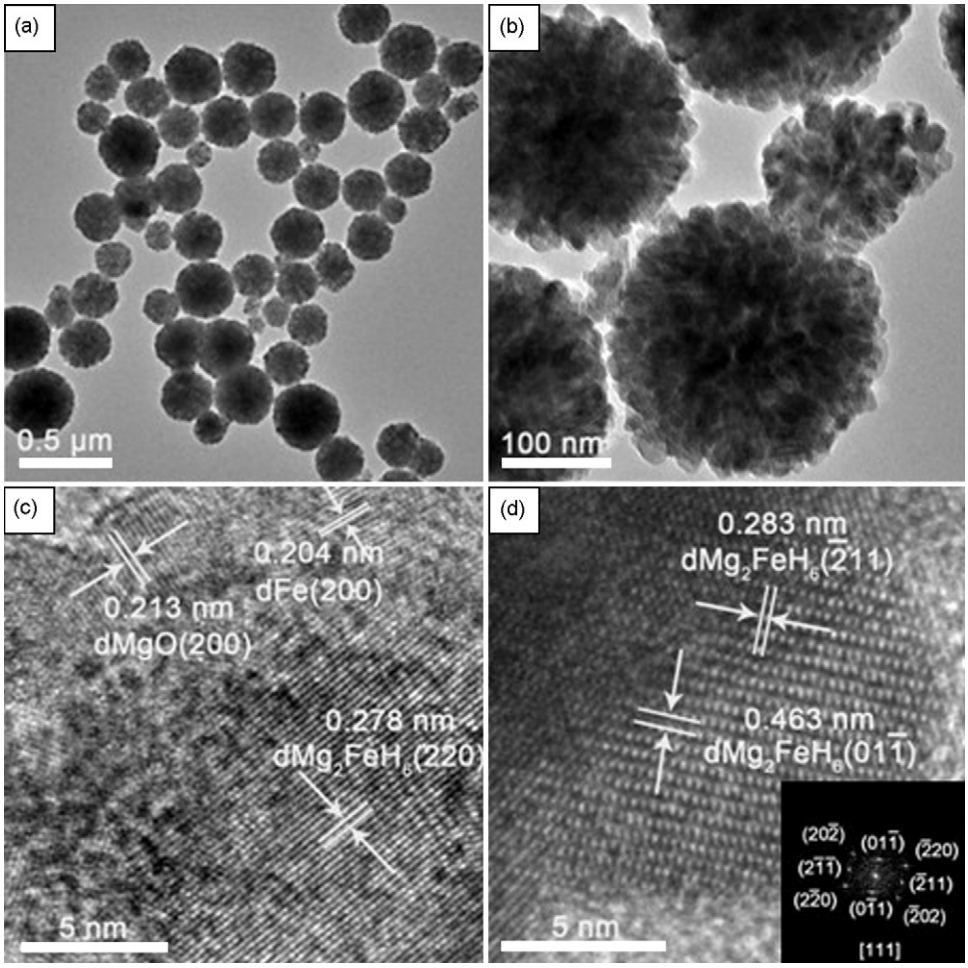


**Fig. 3.** Structural analysis of the product prepared by ball milling the 3Mg + Fe mixture for 100 h at the hydrogen pressure of 5.5 bar: (a and b) TEM; (c and d) HRTEM images. The inset of (d) is the corresponding fast Fourier transform (FFT) patterns of $Mg_2FeH_6$.

1.484 bar), (548 K, 0.672 bar), and (523 K, 0.384 bar). Fig. 7 shows the van't Hoff plot for the obtained $Mg_2FeH_6$ samples. From Fig. 7, the decomposition enthalpies and entropies of $Mg_2FeH_6$ are calculated, as summarized in Table 2. The decomposition enthalpy and entropy for the as-prepared $Mg_2FeH_6$ are $-67.2 \pm 8$ kJ/mol $H_2$ and $-120.1 \pm 15$ J/K mol $H_2$, respectively. Compared to the reported results, we can see that the absolute values of the present

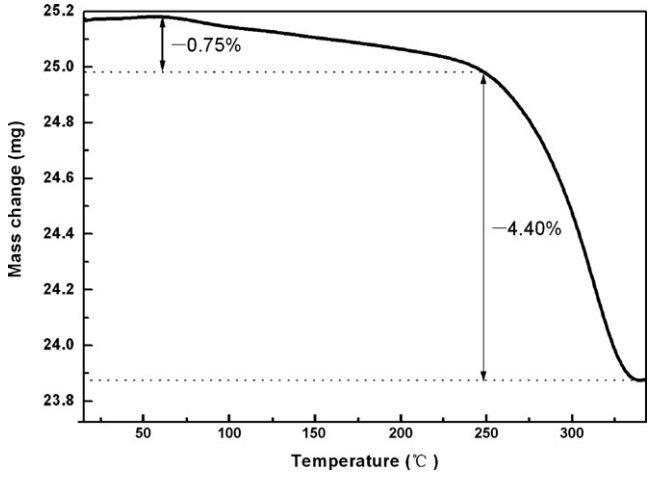


**Fig. 4.** TG curve of the as-prepared $Mg_2FeH_6$ under vacuum.

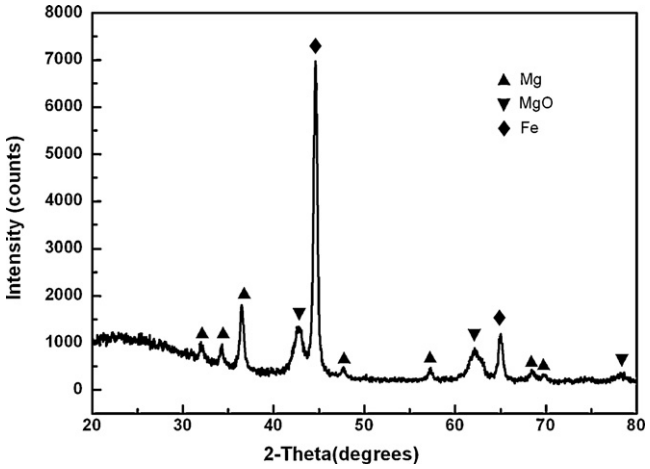


**Fig. 5.** The XRD curve for the dehydrogenated $Mg_2FeH_6$.

**Table 2**
The decomposition enthalpy and entropy of the obtained $Mg_2FeH_6$ samples calculated from the van't Hoff plot.

| No. | Enthalpy ($\Delta H$) (kJ/mol $H_2$) | Entropy ($\Delta S$) (J/K mol $H_2$) | Reference |
|---|---|---|---|
| 1 | $-67.2 \pm 8$ | $-120.1 \pm 15$ | This work |
| 2 | $-80 \pm 28$ | $-137 \pm 13$ | [5] |
| 3 | $-87 \pm 3$ | $-147 \pm 15$ | [18] |
| 4 | $-86 \pm 6$ | $-147 \pm 9$ | [8] |
| 5 | $-82.4 \pm 5.8$ | $-140.2 \pm 8.7$ | [14] |

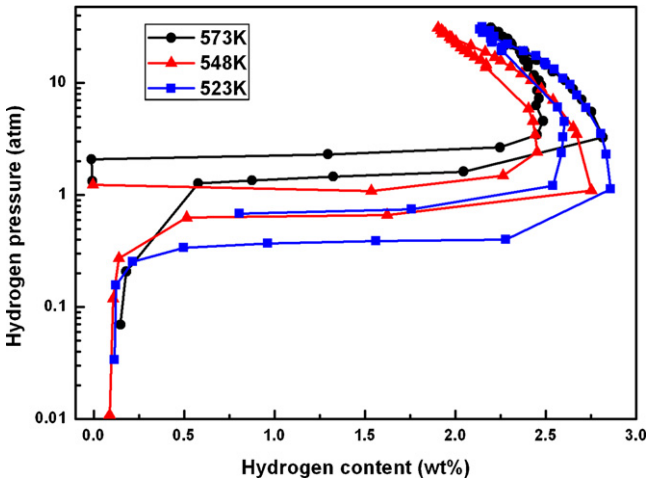


**Fig. 6.** The P–C–T curves of the obtained nanocrystalline $Mg_2FeH_6$ at 573, 548 and 523 K, respectively.

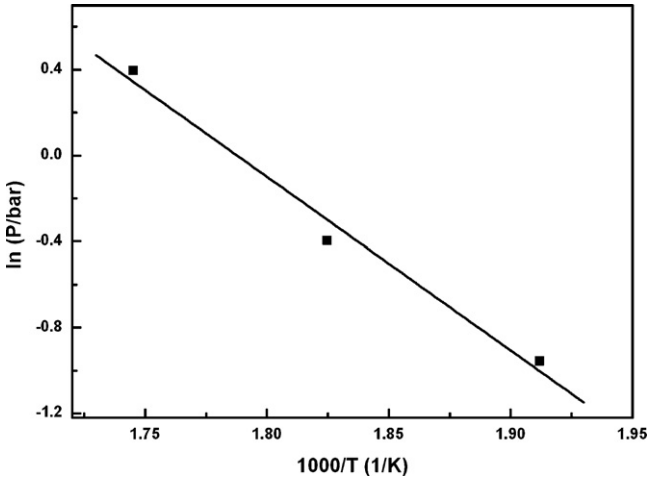


**Fig. 7.** The van't Hoff plot for the nanocrystalline $Mg_2FeH_6$ samples.

enthalpy and entropy are some lower, indicating that nanostructured $Mg_2FeH_6$ shows favorable thermodynamics.

## 4. Conclusions

In summary, we have prepared high proportion of nanocrystalline $Mg_2FeH_6$ by ball milling of 3Mg + Fe mixture under relatively lower hydrogen pressure and room temperature. The sample desorbs up to 5.15 wt% of hydrogen under vacuum from 335 to 613 K with a desorption enthalpy of $-67.2 \pm 8$ kJ/mol $H_2$. In addition, we have also observed the chrysanthemum-like nanostructure composed of aggregated $Mg_2FeH_6$. Viewing down the [1 1 1] zone axis, the nanocrystal $Mg_2FeH_6$ is spherical and the diameter is approximately 10 nm. The present preparation of nanocrystalline $Mg_2FeH_6$ should shed light on making it possible to be further applied as hydrogen-storage materials.

## Acknowledgments

This work was supported by the Research Programs of NSFC (50771056), MOST (2007AA05Z149 and 2009AA03Z224), and MOE (IRT-0927).

## References

[1] B. Peng, J. Chen. Coordin. Chem. Rev. 253 (2009) 2805–2813.
[2] Q. Li, J. Liu, K.C. Chou, G.W. Lin, K.D. Xu, J. Alloys Compd. 466 (2008) 146–152.
[3] H.Y. Shao, T. Liu, Y.T. Wang, H.R. Xu, X.G. Li, J. Alloys Compd. 465 (2008) 527–533.
[4] I.G. Fernandez, G.O. Meyer, F.C. Gennari, J. Alloys Compd. 464 (2008) 111–117.
[5] J.A. Puszkiel, P.A. Larochette, F.C. Gennari, J. Alloys Compd. 463 (2008) 134–142.
[6] R.A. Varin, S.H. Li, Z. Wronski, O. Morozova, T. Khomenko, J. Alloys Compd. 390 (2005) 282–296.
[7] J.J. Didisheim, P. Zolliker, K. Yvon, J. Fischer, M. Gubelmann, Inorg. Chem. 23 (1984) 1953–1957.
[8] P. Selvam, K. Yvon, Int. J. Hydrogen Energy 16 (1991) 615–617.
[9] J. Hout, S. Boily, E. Akiba, J. Alloys Compd. 280 (1998) 306–309.
[10] F.C. Gennari, F.J. Castro, J. Alloys Compd. 339 (2002) 261–267.
[11] R.A. Varin, S.L. Li, Ch. Chiu, L. Guo, O. Morozova, T. Khomenko, Z. Wronski, J. Alloys Compd. 390 (2005) 282–296.
[12] S.S. Sai Raman, D.J. Davidson, J.L. Bobet, O.N. Srivastava, J. Alloys Compd. 333 (2002) 282–290.
[13] L. George, V. Drozd, A. Durygin, J.H. Chen, S.K. Saxena, Int. J. Hydrogen Energy 34 (2009) 3410–3416.
[14] X.Z. Zhang, Y. Yang, J. Qu, W. Zhao, L. Xie, W.H. Tian, X.G. Li, Nanotechnology 21 (2010) 095706.
[15] H. Ma, S.Y. Zhang, W.Q. Ji, Z.L. Tao, J. Chen, J. Am. Chem. Soc. 130 (2008) 5361–5367.
[16] R.A. Young, The Rietveld Method, Oxford University Press, Oxford, 1993 (Chapter 1).
[17] Y. Song, W.C. Zhang, R. Yang, Int. J. Hydrogen Energy 34 (2009) 1389–1398.
[18] J.A. Puszkiel, P.A. Larochette, F.C. Gennari, Int. J. Hydrogen Energy 33 (2008) 3555–3560.